CORRELATION MATRIX INTERPOLATION IN SOUND SOURCE LOCALIZATION FOR A ROBOT

Keisuke Nakamura, Kazuhiro Nakadai, Hirofumi Nakajima, and Gökhan Ince

Honda Research Institute Japan Co., Ltd.
8-1 Honcho, Wako, Saitama, 351-0114, Japan
keisuke@jp.honda-ri.com, nakadai@jp.honda-ri.com,
nakajima@jp.honda-ri.com, gokhan.ince@jp.honda-ri.com

ABSTRACT

In microphone array processing, a Correlation Matrix (CM) between multiple channel input signals is widely utilized for various purposes such as Sound Source Localization (SSL), etc. The CM corresponds to spatial information between a microphone and a sound source, and it dynamically changes as they move in a dynamic environment. Since pre-measured CMs have difficulties in dealing with dynamically changing environments due to their discreteness, this paper addresses a CM interpolation utilizing a few discrete known CMs. The proposed method is based on an integration of eigen-value-scaling and linear interpolation, which requires a few measurements and low computational costs. Apart from conventional methods, this paper deals with an interpolation based on a *correlation-matrix* not based on a transfer-function, which achieves the integration approach. The evaluation shows better estimation performance compared to conventional transfer-function-based methods. We also applied the interpolation to SSL and confirmed its validity.

Index Terms— Robot Audition, Sound Source Localization, Correlation Matrix Interpolation

1. INTRODUCTION

Acoustic signal processing with a microphone array has been widely investigated and applied to robot audition for a decade. In the process, a *Correlation Matrix (CM)* of multiple channel input signals which corresponds to a *Spatial Transfer Function (STF)* plays an important role for a variety of purposes such as *Sound Source Localization (SSL)*, sound source separation, etc.

For instance, we use CMs in the previously reported Generalized-Eigen-Value-Decomposition-based Multiple SIgnal Classification (GEVD-MUSIC)[1] as

$$\boldsymbol{R}\boldsymbol{e}_m = \lambda_m \boldsymbol{K}\boldsymbol{e}_m \ , \tag{1}$$

where $\boldsymbol{R}$ and $\boldsymbol{K}$ are a signal CM and a freely designable CM, and λ_m and $\boldsymbol{e}_m$ are their eigen values and vectors, respectively. In GEVD-MUSIC, the spatial spectrum for a Direction of Arrival (DoA) estimation is described as

$$P(\psi) = \frac{|\boldsymbol{G}^*(\psi)\boldsymbol{G}(\psi)|}{\sum_{m=L+1}^{M} |\boldsymbol{G}^*(\psi)\boldsymbol{e}_m|} \ , \tag{2}$$

where $\boldsymbol{G}$ is the steering vector, ψ is DoA to be estimated. Since (2) only includes $\boldsymbol{e}_m$ as a variable, the selection of $\boldsymbol{e}_m$ in (1) drastically affects the SSL performance. Therefore, $\boldsymbol{K}$ should be properly designed.

With robot-embedded microphones, both microphones and sound sources move dynamically. In this case, $\boldsymbol{K}$ should be adaptable to the movement since the geometrical relationship between a source and an array is changed. The problem is that , in contrast to the continuous change of the geometrical relationship, it is hard to estimate $\boldsymbol{K}$ with the change.

For the continuous estimation of $\boldsymbol{K}$, several *transfer-function-based* methods have been reported, which are mainly categorized into two approaches, *blind methods* and *semi-blind methods*. The blind methods such as BEM [2] and the scattering theory [3] numerically derive continuous STFs. However, they require high computational power, and it is difficult for them to achieve real-time estimation which we require for robot applications. The semi-blind methods utilize several pre-measured discrete STFs and achieve a low computational cost compared to blind methods. The methods can be categorized into *indirect methods* and *direct methods*. The indirect methods [4-11] utilize all the known STFs to estimate one, which realizes high estimation accuracy. However, their computational cost still has difficulties in real-time implementation for robots. On the other hand, the direct methods [12-14] utilize only the two closest pre-measured STFs from the estimated point. Therefore, they have advantages regarding real-time implementation. Therefore, this paper focuses on a low computational direct method. However, the low estimation accuracy problem still remains.

To solve the issue, this paper proposes hybrid CM estimation approach based on the integration of an eigen-value-scaling approach and a linear interpolation approach. The integration works to reduce the estimation error for both magnitude and phase. Despite numerous publications about inter-

Table 1. Notation of Variables

M	Number of microphones
m	Microphone index ($1 \leq m \leq M$)
$\hat{\phi}$	Position/direction of an estimated point
ϕ_1, ϕ_2	Two closest position/direction from $\hat{\phi}$
$A_m(\phi)$	STF between a source and the m-th microphone
$\hat{A}_m(\phi)$	Estimated $A_m(\phi)$
$\boldsymbol{A}(\phi)$	$[A_1(\phi), ..., A_M(\phi)]^T \in \mathbb{C}^M$
$\hat{\boldsymbol{A}}(\phi)$	$[\hat{A}_1(\phi), ..., \hat{A}_M(\phi)]^T \in \mathbb{C}^M$
$a_m(t, \phi)$	Time domain representation of $A_m(\phi)$
$\hat{a}_m(t, \phi)$	Estimated $a_m(t, \phi)$
D_A	A scaling factor for interpolation
$\boldsymbol{\mathcal{A}}(\phi)$	CM obtained by $\boldsymbol{A}(\phi)$. $\boldsymbol{\mathcal{A}}(\phi) \in \mathbb{C}^{M \times M}$
$\hat{\boldsymbol{\mathcal{A}}}_{[\phi_1,\phi_2]}(\hat{\phi})$	Estimated $\boldsymbol{\mathcal{A}}(\hat{\phi})$ using $\boldsymbol{\mathcal{A}}(\phi_1)$ and $\boldsymbol{\mathcal{A}}(\phi_2)$

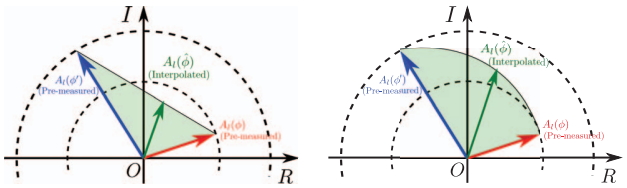

(a) FDLI method (b) TDLI method

Fig. 1. Intuitive Image of Interpolation

polation, the difference is that we are interested in the interpolation of *correlation matrices* not transfer functions. The matrix problem formulation has an advantage in decoupling an estimated CM into amplitude and phase and realizes the hybrid approach. We also show the application of the estimation through SSL.

2. RELATED WORK

All the notation of variables is listed in Table 1. Here, Frequency Domain Linear or bi-linear Interpolation (**FDLI**) [7, 12, 13] and Time Domain Linear Interpolation (**TDLI**) [14] are specifically investigated.

FDLI methods have $\boldsymbol{A}(\phi_1) = [A_1(\phi_1), \ldots, A_M(\phi_1)]^T$ and $\boldsymbol{A}(\phi_2) = [A_1(\phi_2), \ldots, A_M(\phi_2)]^T$ as pre-measured spatial transfer functions, where M is the number of microphones, ϕ_1 and ϕ_2 are the pre-measured direction. The objective is to estimate $\boldsymbol{A}(\hat{\phi})$ by interpolation, where $\phi_1 < \hat{\phi} < \phi_2$. The linear interpolation in the frequency domain can be obtained by the following equation [7].

$$\hat{\boldsymbol{A}}(\hat{\phi}) = D_A \boldsymbol{A}(\phi_1) + (1 - D_A)\boldsymbol{A}(\phi_2) \,, \tag{3}$$

where $\hat{\boldsymbol{A}}$ is the estimated transfer function ($\boldsymbol{A}$ is the correct one), and $D_A \in \mathbb{R}$ is a scalar which is $0 \leq D_A \leq 1$. Fig. 1(a) shows the intuitive image of the interpolation between two transfer functions. As seen in the figure, magnitude estimation is less focused than that for phase. This method is extended for the *correlation matrix* interpolation as follows:

$$\hat{\boldsymbol{\mathcal{A}}}_{[\phi_1,\phi_2]}(\hat{\phi}) = \hat{\boldsymbol{A}}(\hat{\phi})\hat{\boldsymbol{A}}^*(\hat{\phi}) \,, \tag{4}$$

where $()^*$ is a complex conjugate transpose operator.

TDLI is described as follows:

$$a_m(t + d_{\hat{\phi}}, \hat{\phi}) = \frac{k_{\phi_2} a_m(t + d_{\phi_2}, \phi_2) + k_{\phi_1} a_m(t + d_{\phi_1}, \phi_1)}{k_{\phi_2} + k_{\phi_1}} \tag{5}$$

$$d_{\hat{\phi}} = \frac{k_{\phi_2} d_{\phi_2} + k_{\phi_1} d_{\phi_1}}{k_{\phi_2} + k_{\phi_1}} \,, \tag{6}$$

where k_{ϕ_1} and k_{ϕ_2} are geometrically determined weights, d_{ϕ_1} and d_{ϕ_2} are geometrical time delay, and $a_m(t, \hat{\phi})$ is $A_m(\hat{\phi})$ in the time domain ($1 \leq m \leq M$). (5) is considered as amplitude interpolation, and (6) describes a time interpolation. In the frequency domain, the interpolation is regarded as an interpolation of both magnitude and phase. Therefore the method interpolates transfer functions like Fig. 1(b). From (5) and (6), $\hat{\boldsymbol{A}}(\hat{\phi}) = [\hat{A}_1(\hat{\phi}), \ldots, \hat{A}_M(\hat{\phi})]^T$ is determined as follows in the frequency domain:

$$\hat{A}_m(\hat{\phi}) = A_m(\phi_2)(A_m(\phi_1)/A_m(\phi_2))^{D_A} \,. \tag{7}$$

Finally, with (7), the interpolation is obtained by (4).

Both FDLI and TDLI methods can interpolate transfer functions from $\boldsymbol{A}(\phi_1)$ to $\boldsymbol{A}(\phi_2)$ continuously in a short time by the factor D_A. However, they have less interpolation accuracy compared to indirect ones. In order to achieve high accuracy, the next session proposes a direct method based on the eigen-value-scaling approach which is suitable for robots.

3. EIGEN-VALUE-SCALING APPROACH

This section describes the details of the proposed integration method between the Eigen-Value-Scaling (EVS) approach and linear interpolation approach. We firstly introduce two preliminary EVS approaches, that is, M-EVSI in Section 3.1 and S-EVSI in Section 3.2. After that, the details of the integration method are described in Section 3.3.

3.1. Multiplication-based EVS Interpolation (M-EVSI)

The idea is to scale the eigen values of the CM and connect two CMs smoothly. The CM is interpolated as follows:

1) Take two known CMs in the directions of ϕ_1 and ϕ_2, namely $\boldsymbol{\mathcal{A}}(\phi_1)$ and $\boldsymbol{\mathcal{A}}(\phi_2)$, where

$$\boldsymbol{\mathcal{A}}(\phi) = \boldsymbol{A}(\phi)\boldsymbol{A}^*(\phi) \tag{8}$$

2) Define $\boldsymbol{\mathcal{A}}_T(\phi_1, \phi_2) = \boldsymbol{\mathcal{A}}(\phi_1)\boldsymbol{\mathcal{A}}^{-1}(\phi_2)$
3) Take EVD of $\boldsymbol{\mathcal{A}}_T(\phi_1, \phi_2)$ by $\boldsymbol{\mathcal{A}}_T(\phi_1, \phi_2) = \boldsymbol{E}_T \boldsymbol{\Lambda}_T \boldsymbol{E}_T^{-1}$.
4) Calculate the interpolated matrix $\hat{\boldsymbol{\mathcal{A}}}_{[\phi_1,\phi_2]}(\hat{\phi})$.

$$\hat{\boldsymbol{\mathcal{A}}}_{[\phi_1,\phi_2]}(\hat{\phi}) = \boldsymbol{\mathcal{A}}(\phi_2)\boldsymbol{E}_T \boldsymbol{\Lambda}_T^{D_A} \boldsymbol{E}_T^{-1} \,. \tag{9}$$

When $D_A = 0$ in (9), $\hat{\boldsymbol{\mathcal{A}}}_{[\phi_1,\phi_2]}(\hat{\phi}) = \boldsymbol{\mathcal{A}}(\phi_2)$, and $D_A = 1$ induces $\hat{\boldsymbol{\mathcal{A}}}_{[\phi_1,\phi_2]}(\hat{\phi}) = \boldsymbol{\mathcal{A}}(\phi_1)$. Therefore, the smooth change of D_A from 0 to 1 realizes interpolation of the CM from ϕ_1 to ϕ_2.

3.2. Subtraction-based EVS Interpolation (S-EVSI)

Subtraction-based interpolation can be defined with few modifications. The S-EVSI algorithm is as follows:

1) Take two known CMs, $\boldsymbol{\mathcal{A}}(\phi_1)$ and $\boldsymbol{\mathcal{A}}(\phi_2)$.

$$\boldsymbol{\mathcal{A}}(\phi) = \boldsymbol{A}(\phi)\boldsymbol{A}^*(\phi) \tag{10}$$

2) Take two EVDs for both $\boldsymbol{\mathcal{A}}(\phi_1)$ and $\boldsymbol{\mathcal{A}}(\phi_2)$ by $\boldsymbol{\mathcal{A}}(\phi_1) = \boldsymbol{E}_{\phi_1}\boldsymbol{\Lambda}_{\phi_1}\boldsymbol{E}_{\phi_1}^{-1}$ and $\boldsymbol{\mathcal{A}}(\phi_2) = \boldsymbol{E}_{\phi_2}\boldsymbol{\Lambda}_{\phi_2}\boldsymbol{E}_{\phi_2}^{-1}$

3) Calculate the interpolated matrix $\hat{\boldsymbol{\mathcal{A}}}_{[\phi_1,\phi_2]}(\hat{\phi})$ as follows:

$$\hat{\boldsymbol{\mathcal{A}}}_{[\phi_1,\phi_2]}(\hat{\phi}) = \boldsymbol{E}_{\phi_2}\boldsymbol{\Lambda}_{\phi_2}^{1-D_A}\boldsymbol{E}_{\phi_2}^{-1} + \boldsymbol{E}_{\phi_1}\boldsymbol{\Lambda}_{\phi_1}^{D_A}\boldsymbol{E}_{\phi_1}^{-1} - \boldsymbol{I}\ , \tag{11}$$

where $\boldsymbol{I} \in \mathbb{R}^{M\times M}$ is an identity matrix.

The same as M-EVSI, the change of D_A from 0 to 1 interpolates $\hat{\boldsymbol{\mathcal{A}}}_{[\phi_1,\phi_2]}(\hat{\phi})$ from $\boldsymbol{\mathcal{A}}(\phi_2)$ to $\boldsymbol{\mathcal{A}}(\phi_1)$ smoothly.

3.3. Integration Methodology

Up to here, we described four methods, FDLI, TDLI, M-EVSI, and S-EVSI. For CMs, the estimation of eigen values and eigen vectors is important since they roughly represent magnitude and phase. Therefore, the idea of integration is to select eigen vectors and eigen values from different methods which have the best interpolation performance. Here, eigen vectors of *FDLI* and eigen values of *M-EVSI* are selected as the following integration:

1) Take two interpolation results from (4) and (9). Here, $\hat{\boldsymbol{\mathcal{A}}}_{[\phi_1,\phi_2]}(\hat{\phi})$ in (4) and (9) are redefined as $\hat{\boldsymbol{\mathcal{A}}}_{\mathrm{F}[\phi_1,\phi_2]}(\hat{\phi})$ and $\hat{\boldsymbol{\mathcal{A}}}_{\mathrm{M}[\phi_1,\phi_2]}(\hat{\phi})$, respectively.
2) Take EVDs for $\hat{\boldsymbol{\mathcal{A}}}_{\mathrm{F}[\phi_1,\phi_2]}(\hat{\phi})$ and $\hat{\boldsymbol{\mathcal{A}}}_{\mathrm{M}[\phi_1,\phi_2]}(\hat{\phi})$.

$$\hat{\boldsymbol{\mathcal{A}}}_{\mathrm{F}[\phi_1,\phi_2]}(\hat{\phi}) = \boldsymbol{E}_{\mathrm{F}}\boldsymbol{\Lambda}_{\mathrm{F}}\boldsymbol{E}_{\mathrm{F}}^{-1} \tag{12}$$

$$\hat{\boldsymbol{\mathcal{A}}}_{\mathrm{M}[\phi_1,\phi_2]}(\hat{\phi}) = \boldsymbol{E}_{\mathrm{M}}\boldsymbol{\Lambda}_{\mathrm{M}}\boldsymbol{E}_{\mathrm{M}}^{-1}\ . \tag{13}$$

3) Calculate the interpolation $\hat{\boldsymbol{\mathcal{A}}}_{[\phi_1,\phi_2]}(\hat{\phi})$ as follows:

$$\hat{\boldsymbol{\mathcal{A}}}_{[\phi_1,\phi_2]}(\hat{\phi}) = \boldsymbol{E}_{\mathrm{F}}\boldsymbol{\Lambda}_{\mathrm{M}}\boldsymbol{E}_{\mathrm{F}}^{-1}\ . \tag{14}$$

4. EVALUATION

This section shows the validity of the proposed interpolation. Firstly, Section 4.1 evaluates the interpolation error among the methods in Section 2 and Section 3. Section 4.2 raises an application of the method through SSL.

4.1. Evaluation of Interpolation Errors

This section shows the comparison of estimation errors between conventional methods in Section 2 and EVS-based interpolation methods in Section 3. Notice that we consider the error of matrix $\hat{\boldsymbol{\mathcal{A}}}_{[\phi_1,\phi_2]}(\hat{\phi})$ not a single transfer function.

Fig. 2 compares the estimation errors. The horizontal axis shows the difference between ϕ_1 and ϕ_2, so a larger value is more difficult to estimate. Here, ϕ_1 is fixed at 0°, and ϕ_2 is changed from 10° to 120°. For error calculation, we have measured spatial transfer functions $\boldsymbol{A}(\hat{\phi})$ every 5°, which are obtained by Time-Stretched Pulse recording by a robot embedded microphone array. Therefore, the CM for $\hat{\phi}$ is estimated by 5°. The average error $\bar{e}_{[\phi_1,\phi_2]}$ is calculated as

$$\bar{e}_{[\phi_1,\phi_2]} = \sum_{i=1}^{\phi_2/5-1} \frac{f_{[\phi_1,\phi_2]}(\hat{\phi})}{\phi_2/5-2}\Big|_{\hat{\phi}=5i}\ , \tag{15}$$

where $f_{[\phi_1,\phi_2]}(\hat{\phi})$ is the estimation error. For $f_{[\phi_1,\phi_2]}(\hat{\phi})$, two cases were considered. One is the summation of inner products of eigen vectors calculated as follows:

$$f_{[\phi_1,\phi_2]}(\hat{\phi}) = \sum_{i=1}^{M}\left|\frac{\hat{\boldsymbol{e}}_{\hat{\phi}i}\cdot\boldsymbol{e}_{\hat{\phi}i}}{||\hat{\boldsymbol{e}}_{\hat{\phi}i}||\cdot||\boldsymbol{e}_{\hat{\phi}i}||} - 1\right|\ , \tag{16}$$

where $\boldsymbol{e}_{\hat{\phi}i}$ is the i-th eigen vector of $\boldsymbol{\mathcal{A}}(\hat{\phi})$, and $\hat{\boldsymbol{e}}_{\hat{\phi}i}$ is the i-th eigen vector of $\hat{\boldsymbol{\mathcal{A}}}(\hat{\phi})$ (Namely, $\boldsymbol{E}_{\hat{\phi}} = [\boldsymbol{e}_{\hat{\phi}1},\ldots,\boldsymbol{e}_{\hat{\phi}M}]^T$). The other is an inverse-matrix-based error defined as follows:

$$f_{[\phi_1,\phi_2]}(\hat{\phi}) = \left|\left|\boldsymbol{\mathcal{A}}(\hat{\phi})\hat{\boldsymbol{\mathcal{A}}}_{[\phi_1,\phi_2]}^{-1}(\hat{\phi}) - \boldsymbol{I}^{M\times M}\right|\right|\ . \tag{17}$$

In Fig. 2, the estimation errors based on (16) and (17) are shown in Fig. 2(a) and 2(b), respectively.

We used eight microphones, so $M = 8$. Therefore, in (16), $f_{[\phi_1,\phi_2]}(\hat{\phi}) \le 16$. In Fig. 2(a), $\bar{e}_{[\phi_1,\phi_2]}$ is approximately $3 \le \bar{e}_{[\phi_1,\phi_2]} \le 4.5$ in all the estimations. It means that all the methods can estimate the phase of CMs to some extent, which is referred to as the orientation of eigen vectors. The figure also shows that the FDLI has slightly better performance compared to other methods. In Fig. 2(b), the proposed M-EVSI has a much smaller error than that of other methods, which means that the magnitude of CMs, denoted as the eigenvalues of the matrix, fits to $\boldsymbol{A}(\hat{\phi})$. Finally, Fig. 2 shows that the FDLI can estimate the eigen vectors best, and the M-EVSI provides the best estimation for the eigen value. Therefore, interpolation methods for the integration are selected as Section 3.3. As seen, the integration results successfully show low estimation errors for both (16) and (17).

4.2. Application to Smooth Localization

In this section, the estimation described in Section 3 is applied for the smooth DoA localization with GEVD-MUSIC[1]. In order to validate interpolation reliability, $\boldsymbol{K}$ in (1) is designed so that the estimated direction $\hat{\phi}$ has the highest peak in a spatial spectrum, which is realized by the following steps:

1) Take an arbitrary signal S in the frequency domain.
2) Select D_A in (4) and (9), and derive interpolated CM $\hat{\boldsymbol{\mathcal{A}}}_{[\phi_1,\phi_2]}(\hat{\phi})$ by (14).
3) S is virtually reproduced in the direction of $\hat{\phi}$ as follows:

$$\boldsymbol{\mathcal{A}}_S = \hat{\boldsymbol{\mathcal{A}}}_{[\phi_1,\phi_2]}(\hat{\phi})SS^*\ , \tag{18}$$

where $\boldsymbol{\mathcal{A}}_S$ is the reproduced CM.

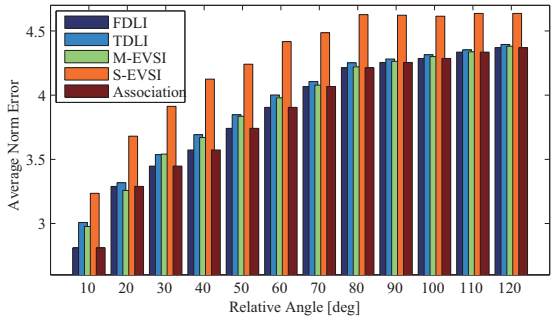

(a) *Error Calculated by (16)*

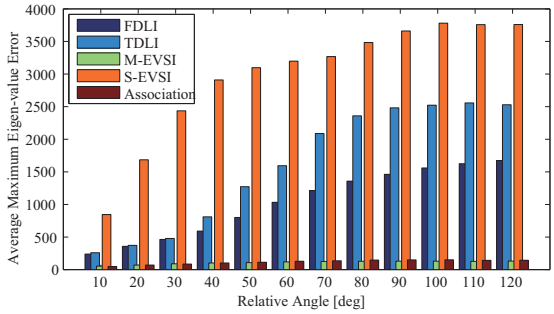

(b) *Error Calculated by (17)*

Fig. 2. *Comparison of Estimation Error*

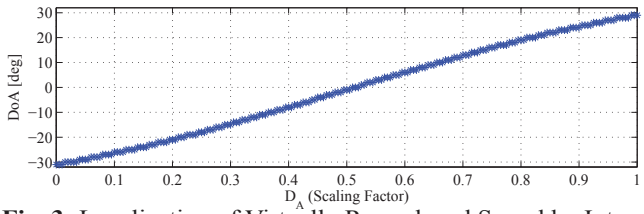

Fig. 3. Localization of Virtually Reproduced Sound by Interpolation

4) Derive $\boldsymbol{R}$ in (1) by a silent source. Ideally, $\boldsymbol{R} = \boldsymbol{I}$.
5) Design $\boldsymbol{K}$ by $\boldsymbol{K} = \boldsymbol{\mathcal{A}}_S^{-1}$
6) Localization by the spatial spectrum by (2)

With the algorithm, (2) ideally localizes the sound in the direction of ϕ. Therefore, reliability of the interpolation can be confirmed by localizing the virtually reproduced sound by known fine transfer functions. We obtained known transfer functions every 1[deg] with offline calculations for precise evaluation (Here, we assume microphones and sounds are in free space). $\phi_1 = 30[\text{deg}], \phi_2 = -30[\text{deg}]$ are adopted.

Fig. 3 shows the results when D_A is changed from 0 to 1. The horizontal axis shows D_A, and the vertical axis represents the DoA results. As seen in the figure, the highest peak moves smoothly from ϕ_2 to ϕ_1 as the D_A changes, and no outlier is detected, which successfully validates the interpolation.

5. CONCLUSION

This paper presented a hybrid CM interpolation method based on eigen-value-scaling and linear interpolation. The method has an advantage of low computational cost and real-time implementation. The proposed approach was compared to conventional transfer-function-based interpolation methods, and the integration approach successfully showed low estimation errors for both the inner products of CM and the norm of a normalized matrix. The proposed method was applied to SSL in a simulated environment, and the interpolation successfully showed the smooth DoA estimation. This paper only showed a SSL application, but this hybrid approach is mathematically quite generic and can be applicable to other related fields. The future work can be an application of the method for a more realistic environment, especially for SSL under moving microphones and multiple sound sources.

6. REFERENCES

[1] K. Nakamura et al., "Intelligent sound source localization for dynamic environments," in *IROS*, 2009, pp. 664–669.

[2] K. Yamamoto et al., "An acoustic simulation for speech interface of humanoid robot," in *Acoust. Soc. of Japan Autumn Meeting*, 2009, pp. 815–818.

[3] K. Nakadai et al., "Applying scattering theory to robot audition system: robust sound source localization and extraction," in *IROS*, 2003, vol. 2, pp. 1147–1152.

[4] D. J. Kistler et al., "A model of head-related transfer functions based on principal components analysis and minimum-phase reconstruction," *J Acoust Soc Am.*, vol. 91, no. 3, pp. 1637–1647, 1992.

[5] L. Wang et al., "Head-related transfer function interpolation through multivariate polynomial fitting of principal component weights," *Acoust. Sci. & Tech.*, vol. 30, no. 6, pp. 395–403, 2009.

[6] T. Nishino et al., "Principal component analysis on head related transfer function," *Tech. Report of the Institure of Electronics Information and Communication Engineers*, vol. 74, no. 49, pp. 1–7, 1996.

[7] T. Nishino et al., "Interpolating head related transfer functions in the median plane," in *Proc. of IEEE WASPAA*, 1999, pp. 167–170.

[8] F. Keyrouz et al., "A rational hrtf interpolation approach for fast synthesis of moving sound," in *the 12th Digital Signal Processing Workshop and 4th Signal Processing Education Workshop*, 2006, pp. 222–226.

[9] T. Ajdler et al., "Plenacoustic function on the circle with application to hrtf interpolation," in *IEEE ICASSP*, 2005, pp. 273–276.

[10] C. I. Cheng et al., "Spatial frequency response surfaces: an alternative visualizationtool for head-related transfer functions (hrtfs)," in *IEEE ICASSP*, 1999, pp. 961–964.

[11] F. P. Freeland et al., "Hrtf interpolation through direct angular parameterization," in *IEEE Int. Symp. on Circ. and Sys.*, 2007, pp. 1823–1826.

[12] K. Watanabe et al., "Interpolation of head-related transfer functions based on the common-acoustical-pole and residue model," *Acoust. Sci. & Tech.*, vol. 24, no. 5, pp. 335–337, 2003.

[13] J. Zhang et al., "A piecewise interpolation method based on log-least square error criterion for hrtf," in *IEEE 7th Workshop on Multimedia Signal Processing*, 2005, pp. 1–4.

[14] M. Matsumoto et al., "A method of interpolating binaural impulse responses for moving sound images," *Acoust. Sci. & Tech.*, vol. 24, no. 5, pp. 284–292, 2003.